Journal of Marine Research, 63, 789–812, 2005

Subantarctic Mode Water and Antarctic Intermediate Water in the South Indian Ocean based on profiling float data 2000–2004

by Annie P. S. Wong[1,2]

ABSTRACT

Autonomous CTD profiling float data from Argo between 2000 and 2004 have been used to study the properties of Subantarctic Mode Water (SAMW) and Antarctic Intermediate Water (AAIW) in relation to local winter mixed layer properties and frontal regimes in the South Indian Ocean. By calculating noise variance at the tightest part of the θ-S curve, the accuracy of salinity in the selected Argo data set has been estimated to be better than 0.01 psu. The basin-wide and seasonally unbiased sampling of the float array shows that South Indian Ocean SAMW is more continuous in geographical and density space than previously observed. Its density and thickness distributions are related to the winter mixed layer properties in the local Subantarctic Zone, with progressively denser and thicker SAMW to the east. The salinity minimum associated with South Indian Ocean AAIW was centered on $\sigma_\theta = 27.2$ kg m^{-3}. As observed by previous hydrographic surveys, fresh AAIW is injected northward into the subtropical gyre in mid-basin, at about 65–85E. Argo profiles show that this northward flow extends to the northern extent of the study region at 15S. In the latitude band 30–40S and east of 55E, meridional salinity gradient on density surfaces in AAIW is the smallest in the South Indian Ocean. Hence that location is the best place in the South Indian Ocean to detect integrated decadal changes in the salinity minimum of AAIW.

1. Introduction

Between 2000 and 2004, more than 200 profiling floats populated the South Indian Ocean as part of the Argo project. Argo is a global array of autonomous conductivity-temperature-depth (CTD) profiling floats that provides vertical profiles of salinity and temperature of the upper 2000 dbar of the open ocean at 10-day intervals (Gould *et al.,* 2004). The advantages of hydrographic sampling by an array of well-dispersed autonomous profiling floats are numerous. Such an array gives continuous synoptic snapshots of water properties in entire basins, as opposed to traditional hydrographic surveys that only give one-time snapshots along single-line transects. Additionally, it samples the seasons evenly, so the measurements are not biased toward seasons favorable for ship-based work.

One disadvantage of sampling by autonomous floats is that most of the measurements

1. JIMAR, SOEST, University of Hawaii, Honolulu, Hawaii, 96822, U.S.A.
2. Present address: School of Oceanography, University of Washington, Seattle, Washington, 98195, U.S.A.
email: awong@ocean.washington.edu

are without accompanying ship-board data for absolute calibration. This deficiency is especially problematic for salinity, as conductivity cells are prone to changes that can cause sensor drift in float salinity measurements. Several methods of calibration are available to adjust sensor drift by comparison with deployment ship-board CTD data or statistical estimates of background θ-S relations (e.g. Bacon *et al.,* 2001; Wong *et al.,* 2003).

Intermediate-depth water masses are a subject of great interest, because they ventilate the thermocline of the subtropical gyres and because they are potential climate change indicators (e.g. Banks *et al.,* 2000). The two main intermediate-depth water masses of the southern hemisphere are Subantarctic Mode Water (SAMW) and Antarctic Intermediate Water (AAIW). SAMW is the product of the thick winter mixed layers in the circumpolar Subantarctic Zone (McCartney, 1977). It is identifiable as a pycnostad with high oxygen content. AAIW is the signature intermediate-depth low salinity tongue that extends equatorward from north of the circumpolar Antarctic Polar Front. The process and location of formation and renewal of AAIW is still an area of debate. McCartney (1977) suggested that AAIW formation involved cooling and overturning of SAMW in the southeast Pacific. Molinelli (1981) suggested that isopycnal mixing of Antarctic Surface Water with waters at depth in the Subantarctic Zone could account for AAIW formation. Sloyan and Rintoul (2001) found that both cross-frontal transformation of Antarctic Surface Water and air-sea exchange at outcropping SAMW resulted in the renewal of AAIW.

Both SAMW and AAIW are transported eastward along the Antarctic Circumpolar Current, as well as advected equatorward, with SAMW overlying AAIW. Circumpolar property studies by McCartney (1982) and Piola and Georgi (1982) have observed large changes in SAMW and AAIW properties among the three oceans: Atlantic, Indian, and Pacific. Within the South Pacific and the South Atlantic, AAIW has received detailed basin-wide description by Reid (1965) and Talley (1996), respectively. In the South Indian Ocean, properties of SAMW and AAIW have been described along 18S by Warren (1981), and along 32S by Toole and Warren (1993) and Fine (1993). However, a basin-wide description is lacking in this region.

This study serves two purposes. Firstly, it demonstrates how the Argo data set can be used effectively in large-scale ocean studies. Careful data selection can screen out float salinity measurements that are suspected of having sensor drift. Simple ensemble statistics can then be used to estimate the accuracy of the selected float salinity data. Thus float salinity data can be used without being subjected to the uncertainties related to adjustment in the absence of an absolute standard. Other large-scale ocean studies that have used Argo data have relied on calibrating float salinity against accurate profiles from ships, and therefore the resulting data are subjected to calibration uncertainties (e.g. Centurioni and Gould, 2004). Secondly, it exploits the fact that a large area of the South Indian Ocean that previously contained sparse and infrequent hydrographic measurements now has concurrent and well-dispersed float measurements, thus presenting an opportunity to study the properties of SAMW and AAIW over the entire basin, and over a limited time period. The first part of this study therefore involves detailed description on float salinity selection and

accuracy estimation. The second part of this study describes properties of SAMW and AAIW in the South Indian Ocean, in relation to local frontal and winter mixed layer regimes.

2. Data

a. Float data selection and quality control

Profiles from all Argo floats operating south of the equator in the South Indian Ocean up until April 2004 were obtained from the Argo Global Data Assembly Centers (http://www.ifremer.fr/coriolis/cdc/argo.htm or http://www.usgodae.org/argo/argo.html). Profiles that did not contain information on position or sampling date, and profiles that did not sample deeper than 110 dbar, were not used in this study. Only float data that passed all Argo real-time tests were used (see http://www.ifremer.fr/coriolis/cdc/argo_rfc.htm). Pressure and temperature measurements from the floats that passed the Argo real-time quality control were assumed to be accurate to 2.4 dbar and 0.002°C, respectively (Seabird calibration accuracy). Float salinity measurements were subjected to additional quality control as described below.

Salinity profiles from individual floats were assembled into time series to examine measurement trends over time. The float salinity series were compared with the background climatology determined by the method of Wong *et al.* (2003). The method of Wong *et al.* (2003) gives weighted least squares fits and associated uncertainties of the float profiles to a background climatology that is estimated from a reference data set. The accuracy of the estimated background climatology depends on the contemporaneity and density of the reference data set. For the South Indian Ocean, the reference data set used was a selected subset of the World Ocean Database 2001 (Conkright *et al.,* 2002), with additional data from the 2002 hydrographic repeat of the South Indian Ocean 32S line conducted on Charles Darwin cruise 139 (CD139, see also Bryden *et al.,* 2003 and McDonagh *et al.,* 2005).

Float series that differed from the Wong *et al.* (2003) weighted least squares fits by more than 2× estimation uncertainties ($\Delta S > 2\delta$) were suspected of being contaminated by sensor malfunction and were subjected to further analysis. This criterion was adopted based on the assumption that the majority of float conductivity sensors was uncontaminated, and that most of the differences between float salinities and climatological estimates were due to the floats sampling real natural variability. Hence the difference had to be greater than 2× estimation uncertainty to suspect a float series. (For example, for a normal random variable, we are 95% confident that the interval ±1.96× standard deviation around the sample mean covers the true value of the mean.) In the South Indian Ocean, climatological salinity estimation uncertainty was in general about 0.01 psu, so differences of more than 0.02 psu were suspect.

For the float series that were suspected of being contaminated, time series of salinity on isotherms over the full profiling depth were examined. Where the majority of the isotherms

(or water masses) showed similar anomalies, then it was concluded that sensor drift or offset was present. The segment of the float series that was contaminated ($\Delta S > 2\delta$) was thus excluded from this study, and the stable segment retained. However, if anomalies were only seen on a small selected group of isotherms (or a particular water mass), then it was concluded that the apparent property changes were due to float migration or real natural variability in the particular water mass (B. King, 2003, personal communication). The float series was then judged as having no sensor error and therefore retained for this study. Of the 254 Argo floats in the South Indian Ocean whose time series were examined, about 3% of the floats showed signs of sensor salinity drift, and about 4% of the floats showed signs of sensor calibration offset.

b. Float salinity measurement accuracy

Ocean measurements contain noise. After passing the Argo real-time quality control and the additional climatological screening for sensor drift or offset, noise in the float salinity measurements is then the result of instrument sampling (small sensor drift and offset that cannot be detected by the Wong *et al.* (2003) climatological comparison method), as well as real ocean spatial and temporal variability. Some of the variability can be eliminated from the noise variance by grouping together nearby float data with common properties, and by looking at isotherms that have the most uniform salinity values. Noise variance of appropriately grouped float salinity on uniform isotherms therefore is mostly instrument sampling noise, and thus is an indication of the accuracy of the selected float salinity data.

How to group nearby float data with common properties is a nontrivial question. One method is to assume that float data within the confines determined by the local spatial decorrelation scales are similar in properties. The spatial decorrelation scales of a region in a data set depend on the separation of the data points, as well as the scales of local variabilities. One can determine an appropriate length scale for a data set by using a scale-dependent method (such as that used in Wong *et al.,* 2003) to map the data back to themselves and then checking the residual statistics. Since the residuals are the difference between the original data and the result of the data being mapped to themselves, they are a good indicator of how well the choice of length scales fits the data. In a good-fit map, the statistical distribution of the residuals should resemble that of the *a priori* noise in the original data. Hence, a set of length scales is considered appropriate if the ratio of the standard deviation of the residuals to the standard deviation of the *a priori* noise in the original data set is close to 1.

Suitability of length scales is also dependent on the water masses. Because this study is focused on intermediate-depth water masses, spatial decorrelation scales on a subset of their density surfaces (σ_θ = 26.6 to 27.2 kg m^{-3}) have been estimated for the selected Argo data set. It was determined that a longitudinal scale of 10° and a latitudinal scale of 5° were most appropriate for the selected Argo South Indian Ocean data set, and all selected float profiles were grouped into 5° × 10° boxes. Visual inspection of these groups of profiles further helped in identifying outlying data points (<1% of the data), which were

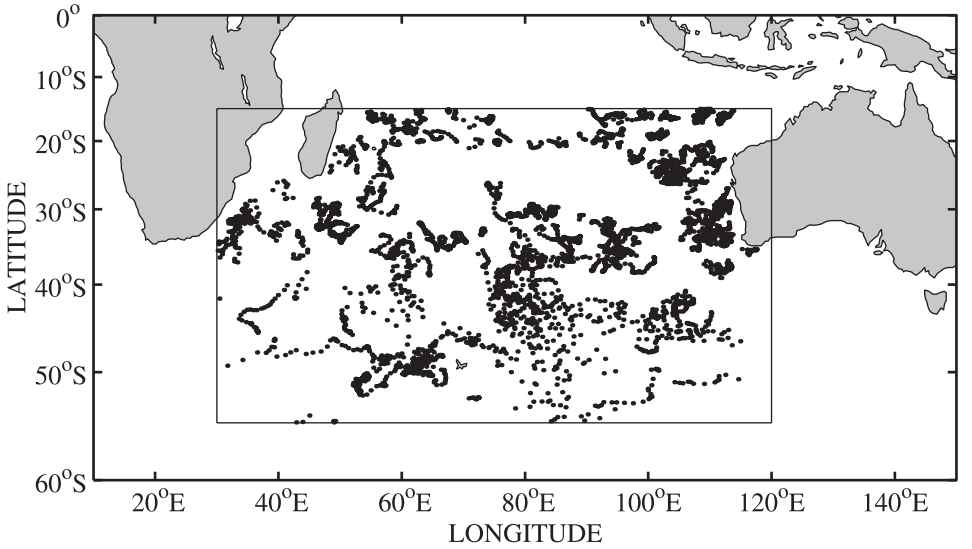

Figure 1. Locations of the 3867 Argo profiles, between May 2000 and April 2004, that were used in this study.

subsequently rejected from this study. At the end, 3867 Argo profiles between 30E and 120E, 15S and 55S, were selected for this study (Fig. 1). These profiles spanned the years 2000 to 2004, and 68% of them sampled deeper than 1000 dbar. North of 15S, the water mass regime is equatorial, and is outside the scope of this study. South of 55S, float measurements were still sparse and as yet inadequate for large-scale studies.

North of 40S, the tightest part of the θ-S curves sampled by Argo floats was between 9°C and 12°C (Fig. 2). Noise variances of salinity interpolated to four isotherms (θ = 11.7°C, 10°C, 9.5°C, 9°C) have thus been calculated for groups of profiles in Figure 2. The noise variance η^2 has been estimated by $\eta^2 = (1/2n)\ \Sigma_i(d_i - d_j)^2$ (Fukumori and Wunsch, 1991), where n is the number of data points on the isotherm in the 5° × 10° box, and d_j is the data point that has the shortest distance from d_i on the isotherm in the 5° × 10° box. This method of estimating the noise variance assumes that noise in each profile is uncorrelated. The isotherm with the smallest value of η, where $\eta = \sqrt{\eta^2}$, is the isotherm with the tightest θ-S relation, and so its η has been taken as the noise of salinity in that box.

South of 40S, the water mass regime is more complex, with multiple water masses on common isotherms. Hence no appropriate isotherms common to profile groups can be used for estimating salinity noise. Instead, salinity noise has been estimated on isopycnal σ_θ = 27.7 kg m^{-3}. Isopycnal σ_θ = 27.7 kg m^{-3} has been chosen because it is one of the deeper isopycnals common to profile groups south of 40S that has minimal spatial variability (Fig. 3). Using isopycnals is less desirable than using isotherms for the purpose of estimating float salinity accuracy, because any error in float salinity will be folded into the calculation for density. However, south of 40S, for a typical water parcel at 1600 dbar with

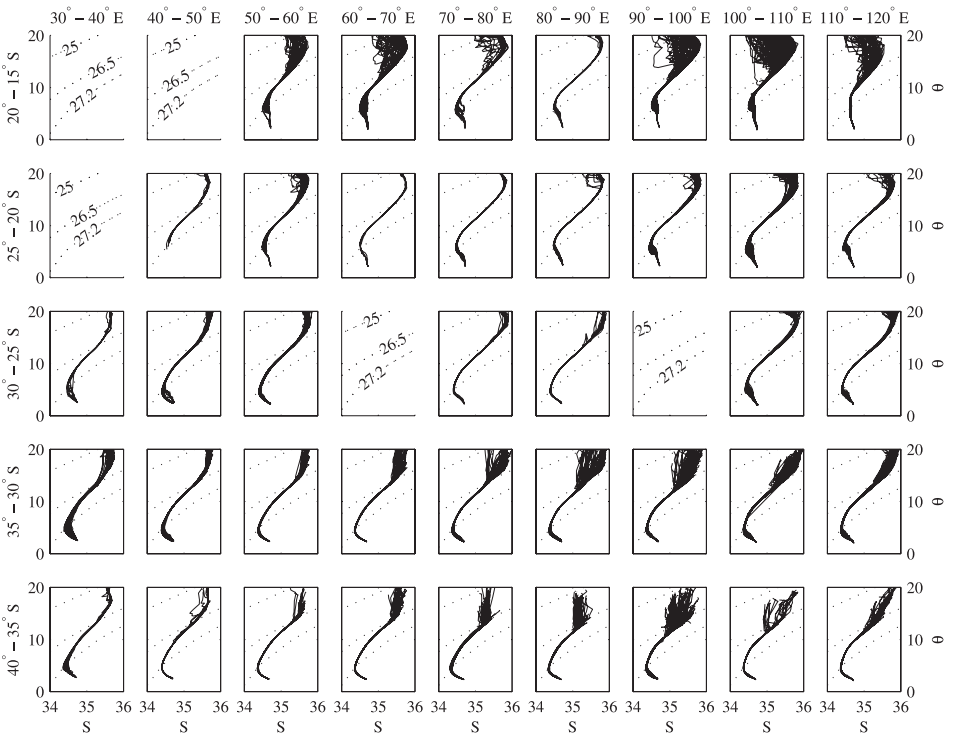

Figure 2. Plots of potential temperature (θ in °C) versus salinity (*S* in PSS-78) of Argo profiles in 5° × 10° boxes between 30E and 120E, 15S and 40S. Contours of σ_θ = 25.0, 26.5, 27.2 kg m^{-3} are superimposed.

potential temperature 2°C and salinity 34.65, salinity error of 0.02 psu will cause less than 0.1% error in the calculation of potential density.

Calculated as such, noise η in the float salinity measurements varied between 0.001 psu and 0.008 psu, with only 20% of the float profile groups having levels above 0.004 psu (Fig. 4). Resolution of float salinity was 0.001 psu. For comparison, contemporaneous CTD data from CD139 between 30S and 35S were grouped and processed in the same manner, yielding noise levels between 0.001 psu and 0.004 psu (Fig. 4d). In all boxes except in 70–80E, salinity measurements from CD139 were less variable than from the Argo profiles. This was, of course, to be expected, since CD139 spanned less than 2 months, while the Argo profiles in this latitude band were collected over more than 2 years. However, it was remarkable that over a period of more than 2 years, the salinity noise level from the Argo floats was not substantially above that from a 2-month CTD cruise.

In addition to considering noise levels, one should also compare measurements from Argo floats with nearby contemporaneous CTD measurements (if available), when

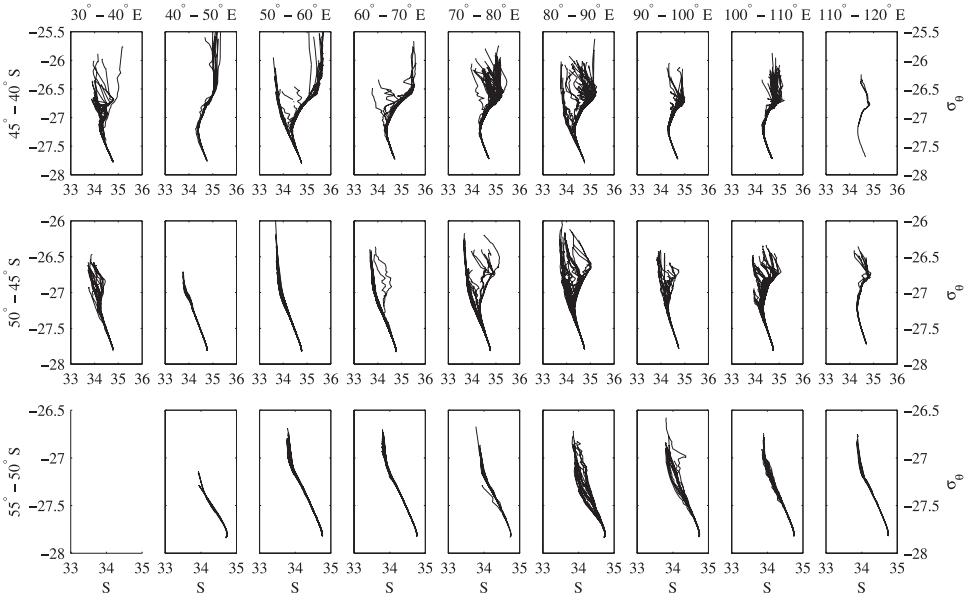

Figure 3. Plots of potential density (σ_θ in kg m^{-3}) versus salinity (S in PSS-78) of Argo profiles in 5° × 10° boxes between 30E and 120E, 40S and 55S.

considering the accuracy of float salinity. For example, in the latitude band 30–35S, on θ = 10°C, mean interpolated salinity from CD139 and from Argo floats (in corresponding 5° × 10° boxes) differed by less than 0.007 psu, except in box 100–110E, where the difference was 0.009 psu. Similar comparison has not been carried out in other latitude bands, because other available CTD measurements in the South Indian Ocean are more than 4 years older than the Argo array, so their measurement differences are likely to contain temporal variability as well as instrument noise. Hence based on noise variance and comparison with CD139, it can be concluded that the estimated salinity accuracy of the Argo data set used in this study is better than 0.01 psu.

3. Circulation, fronts, and winter mixed layer properties in the South Indian Ocean

SAMW and AAIW are both products of the Southern Ocean that are advected into the subtropical gyres of the southern hemisphere. Two fronts mark the boundaries of these water masses and circulation regimes. They are the Subtropical Front (STF) and the Subantarctic Front (SAF). These two fronts, as well as the winter mixed layer properties of the zones delineated by these two fronts, have been identified in the Argo data set. A third front, the Polar Front, which lies poleward of the SAF and is found between approximately 50S and 55S, has not been identified due to the sparsity of data south of 50S in the present data set. The region between the STF and the SAF is referred to as the Subantarctic Zone.

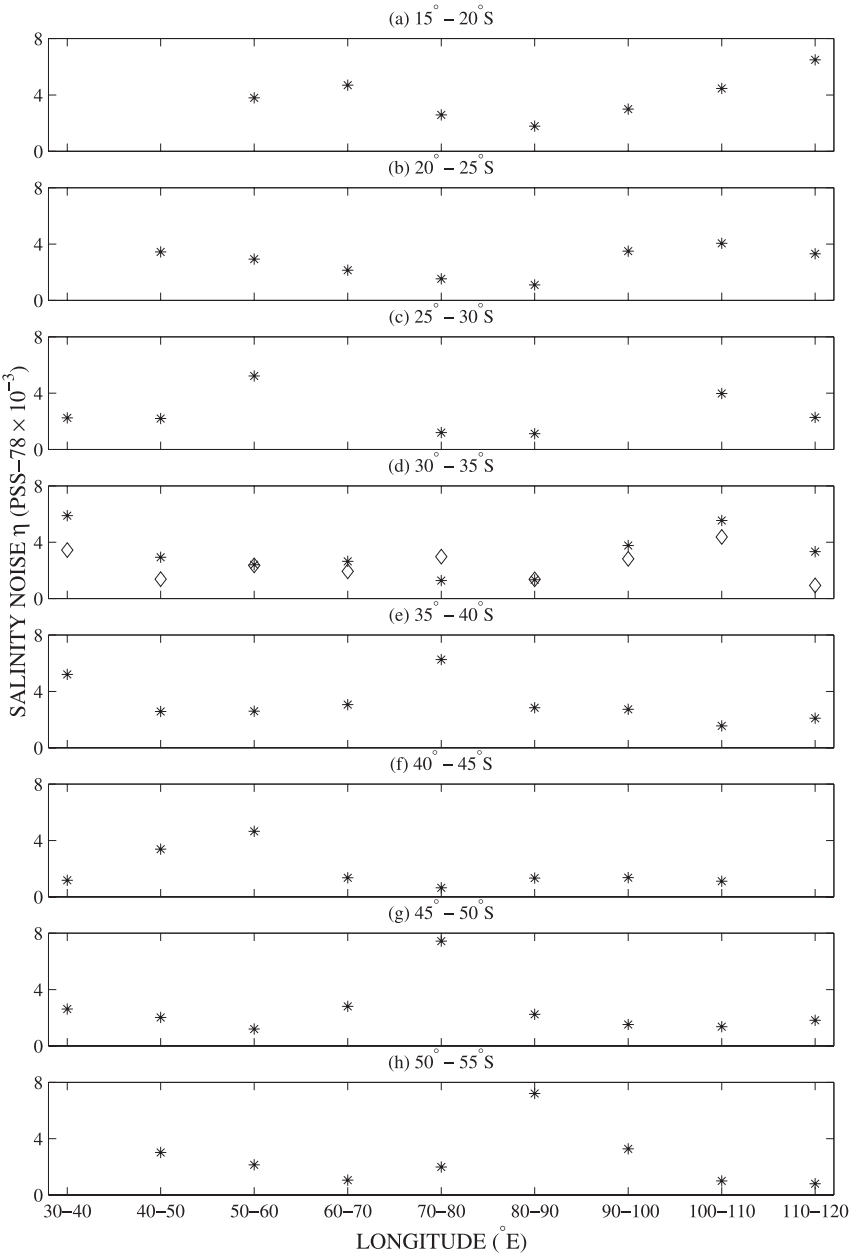

Figure 4. Noise η of interpolated salinity (PSS-78) for profiles in 5° × 10° boxes. * denotes noise from Argo profiles. ◇ denotes noise from CTD profiles from CD139. Noise in (a) to (e) is calculated on the least variable isotherm between 9°C and 12°C. Noise in (f) to (h) is calculated on isopycnal $\sigma_\theta = 27.7$ kg m^{-3}.

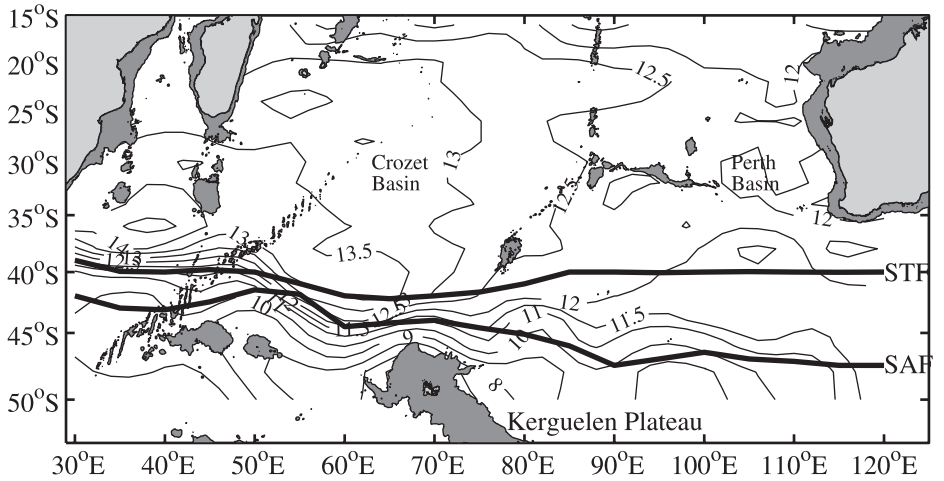

Figure 5. Map of acceleration potential (J kg^{-1}) on $\sigma_\theta = 26.5$ kg m^{-3} relative to 900 dbar. Locations of STF and SAF according to Argo profiles are also shown. Bathymetric regions shallower than 2 km are shaded for identification of geographical features in the South Indian Ocean.

a. Circulation and locations of fronts

The STF and the SAF have been located from float data by hydrographic properties, as in Orsi *et al.* (1995). Equatorward of the STF, at 100 dbar, float profiles have $S > 35.0$ and $\theta > 12$°C. Poleward of the SAF, $S < 34.2$ at 300 dbar, and $\theta < 4$°C at 400 dbar. In addition to this separation by hydrographic properties, float profiles between 40S and 50S, where water mass regime transitions from subtropical to subantarctic (Figs. 2 and 3), have been put through additional visual checking of their θ-S relations to ensure that they have been separated into the correct regimes.

The locations of the STF and the SAF according to Argo profiles (Fig. 5) agree with Stramma (1992) and Orsi *et al.* (1995). In the South Indian Ocean, the STF lies largely along 40S. The SAF lies north of 45S to the west of 80E, but dips poleward of 45S to the east of 80E.

Acceleration potential on $\sigma_\theta = 26.5$ kg m^{-3} relative to 900 dbar has been objectively mapped from the Argo profiles onto a $2° \times 2°$ grid (Fig. 5). Isopycnal $\sigma_\theta = 26.5$ kg m^{-3} has been chosen because it is the lighter density of intermediate-depth water masses in the South Indian Ocean. Contours of acceleration potential on $\sigma_\theta = 26.5$ kg m^{-3} therefore show some of the gross circulation features of these water masses. 900 dbar is the deepest common depth between all Argo profiles.

Equatorward of the STF lies the subtropical gyre of the South Indian Ocean. The westward-flowing South Equatorial Current can be seen in the acceleration potential map at about 15S. A large anticyclonic recirculation cell that may be influenced by local bathymetry (Stramma and Lutjeharms, 1997) exists west of 80E, and provides northward

transport along mid-basin. The eastward-flowing South Indian Ocean Current (SIOC) lies just north of or at the STF, acting as the southern limb of the South Indian Ocean subtropical gyre. It connects with the Agulhas Return Current in the west near South Africa, and turns north upon reaching the southwest coast of Australia (Stramma, 1992). The boundary currents, such as the Agulhas in the western boundary and the Leeuwin in the eastern boundary, are not resolved in the acceleration potential map.

Poleward of the STF lies the eastward-flowing Antarctic Circumpolar Current (ACC). The ACC, and the fronts associated with the ACC (including the SAF), are steered by bottom topography in the Southern Ocean. In the Indian Ocean sector of the Southern Ocean, the most prominent bathymetric obstruction to the ACC is the northwest-to-southeast trending Kerguelen Plateau, lying between 65 and 80E (Fig. 5). North of the Kerguelen Plateau, the SAF and the Polar Front (not identified in this study) often merge (Orsi *et al.,* 1995). Stramma and Lutjeharms (1997) noted that the SIOC and the ACC often merged between 50 and 80E, possibly resulting in an exchange of water masses between the subtropical and the subantarctic regimes. Davis' (2005) study on the mean South Indian circulation using float trajectories at 900 m also showed a significant northward jump of the ACC while passing over the Kerguelen Plateau. The float data clearly show that the Subantarctic Zone, the area between the STF and the SAF, is narrow west of 80E, but widens east of 80E (Fig. 5).

b. Winter mixed layer properties

Properties at the base of the winter mixed layer are described in this section to help infer possible sources for water masses in the South Indian Ocean. Here, the months of August, September and October have been considered as the winter months. The base of the mixed layer has been defined as the pressure at which potential density anomaly σ_θ increases by 0.125 kg m^{-3} from values at 10 dbar. Winter properties have been objectively mapped onto a 2° × 2° grid with spatial decorrelation scales of 10° longitude and 5° latitude (Fig. 6). Very few winter profiles were available south of 35S and west of 50E. Hence properties in that area have not been contoured if objective estimates have large uncertainties.

Winter mixed layer temperature (Fig. 6a) follows a general pattern of decreasing temperature with increasing latitude. The only exception is the higher temperatures south of Madagascar and offshore from the east coast of South Africa, that is due to the influence of the poleward Agulhas Current. Winter mixed layer salinity (Fig. 6b) reflects mostly regional rainfall characteristics. It is highest ($S > 35.6$) between 25 and 35S, because evaporation exceeds precipitation over the subtropical gyre. The northeast corner of the study region east of 100E and equatorward of 20S is an area of strong interannual variability. For example, Phillips *et al.* (2005) have found an average freshening of 0.2 psu, down to 180 m, from 1999 to 2002 in this region, that was believed to be the result of a long-lasting La Niña. Winter mixed layer salinity decreases poleward of the STF, reflecting higher rainfalls over the subantarctic latitudes.

The pattern of winter mixed layer density (Fig. 6c) follows temperature more closely

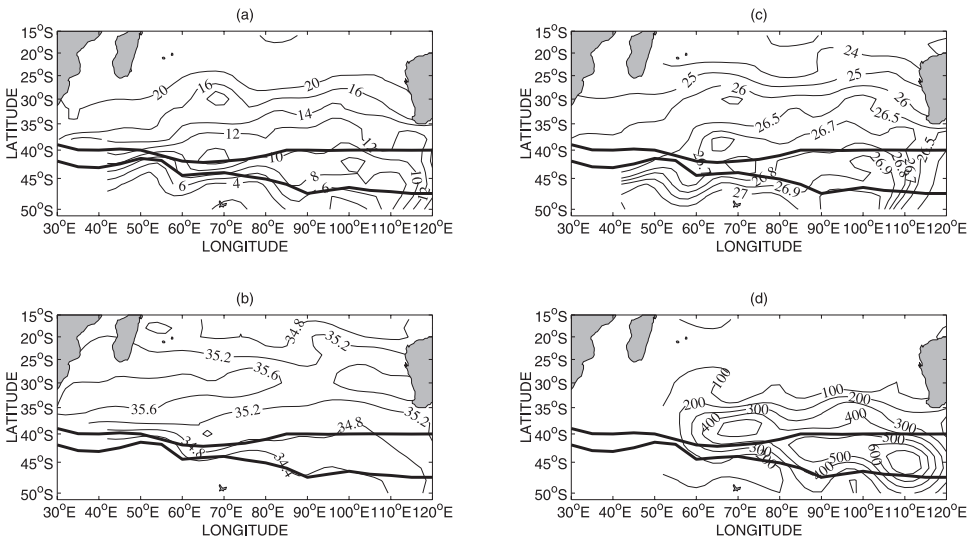

Figure 6. (a) Potential temperature (°C), (b) salinity (PSS-78), (c) potential density (kg m^{-3}), and (d) pressure (dbar), at the base of mixed layer, during months of August, September, and October according to Argo profiles. The two thick lines mark the locations of STF and SAF.

than salinity. In particular, water properties in the Subantarctic Zone are colder and denser towards the east. This is due to the poleward trend of the SAF from the Atlantic to the Indian to the Pacific oceans. The maximum winter mixed layer density in the Indian Subantarctic Zone in the Argo data set is 26.97 kg m^{-3}, with corresponding temperature and salinity of 6.4°C and 34.43, found east of 90E.

Winter mixed layer depths (Fig. 6d) are generally shallower than 200 dbar equatorward of 35S. The Subantarctic Zone east of 80E, where it widens after passing the Kerguelen Plateau, has the thickest, or deepest, winter mixed layers in the South Indian Ocean, with depths exceeding 500 dbar and reaching 800 dbar in places. This result agrees with Talley's (1999) winter mixed layer depth proxy based on 95% oxygen saturation. The cause of this localized increase in winter mixed layer thickness east of the Kerguelen Plateau is still not known (Hanawa and Talley, 2001). Poleward of the SAF, winter mixed layer depths are shallower. There, the highest winter mixed layer density in the Argo data set is 27.47 kg m^{-3}, with corresponding temperature and salinity of −0.56°C and 34.19.

4. Subantarctic Mode Water in the South Indian Ocean

In the South Indian Ocean, according to McCartney (1982), there were two varieties of SAMW. The heavier variety at $\sigma_\theta = 26.85$ mg/cm^3 was thought to originate in the Subantarctic Zone between 100 and 110E. The lighter variety at $\sigma_\theta = 26.70$ mg/cm^3 was thought to originate farther west between 70 and 80E. Fine (1993) observed three density ranges in SAMW along 32S: the lightest SAMW with $\sigma_\theta = 26.5$ kg m^{-3} at 46–62E; a

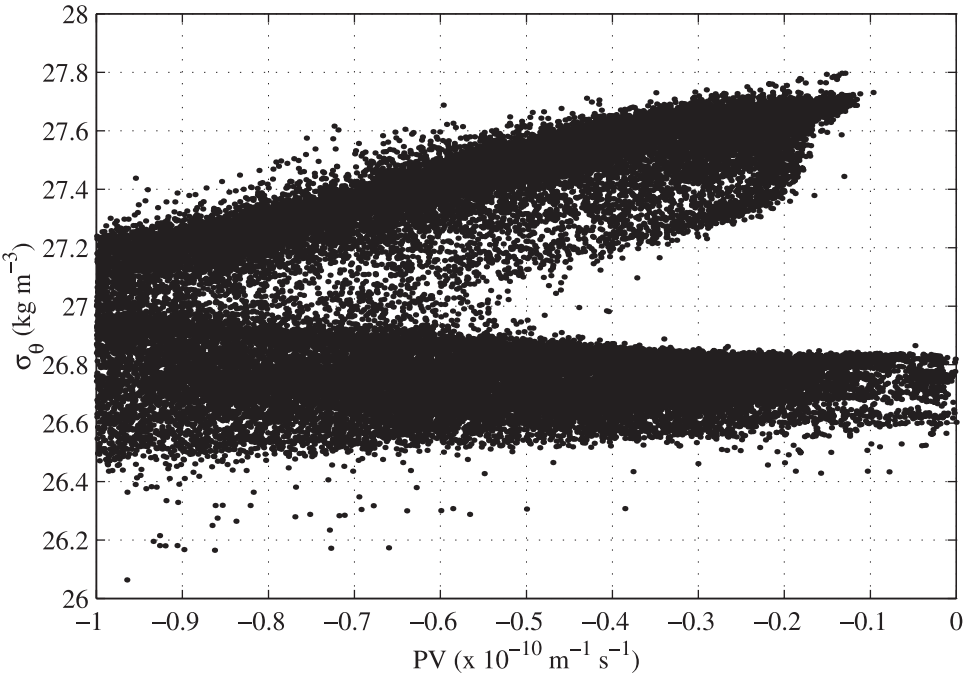

Figure 7. Density range (σ_θ in kg m^{-3}) of waters with planetary potential vorticity $|PV| \leq 1.0 \times 10^{-10}$ m^{-1} s^{-1} that occurred deeper than 200 dbar, north of 45S, in the Argo data set. The lighter layer less than 27.0 kg m^{-3} is SAMW. The denser layer greater than 27.0 kg m^{-3} is AAIW.

SAMW with intermediate density $\sigma_\theta = 26.7$ kg m^{-3} at 72–82E; and the densest SAMW with $\sigma_\theta = 26.8$ kg m^{-3} east of 86E. This densest variety has been referred to as Southeast Indian Subantarctic Mode Water by Talley (1999).

SAMW has been defined in this study as the layer of low planetary potential vorticity $|PV| < 0.5 \times 10^{-10}$ m^{-1} s^{-1} that occurred deeper than 200 dbar but lighter than $\sigma_\theta = 27.0$ kg m^{-3}. The water column above 200 dbar has been excluded to avoid the low PV in the seasonal mixed layer in the subtropical gyre, as well as the subtropical mode water that has been observed near the coast of South Africa (e.g. Gordon *et al.,* 1987; Olson *et al.,* 1992; Toole and Warren, 1993; Fine, 1993). A maximum density of $\sigma_\theta = 27.0$ kg m^{-3} has been set to separate the low PV signature of SAMW from that of the deeper and denser AAIW (Fig. 7).

In the South Indian Ocean, according to this definition, SAMW occupied the density range $\sigma_\theta = 26.5$ to 26.9 kg m^{-3} in the Argo data set. θ-S properties of SAMW (Fig. 8), except for the warmest and saltiest values ($\theta > 13.5$°C and $S > 35.4$), can be found in the winter mixed layer in the local Subantarctic Zone. The warmest and saltiest values were found predominently south of 28S and west of 70E, and were presumably old recirculated SAMW, whose properties had been modified through mixing.

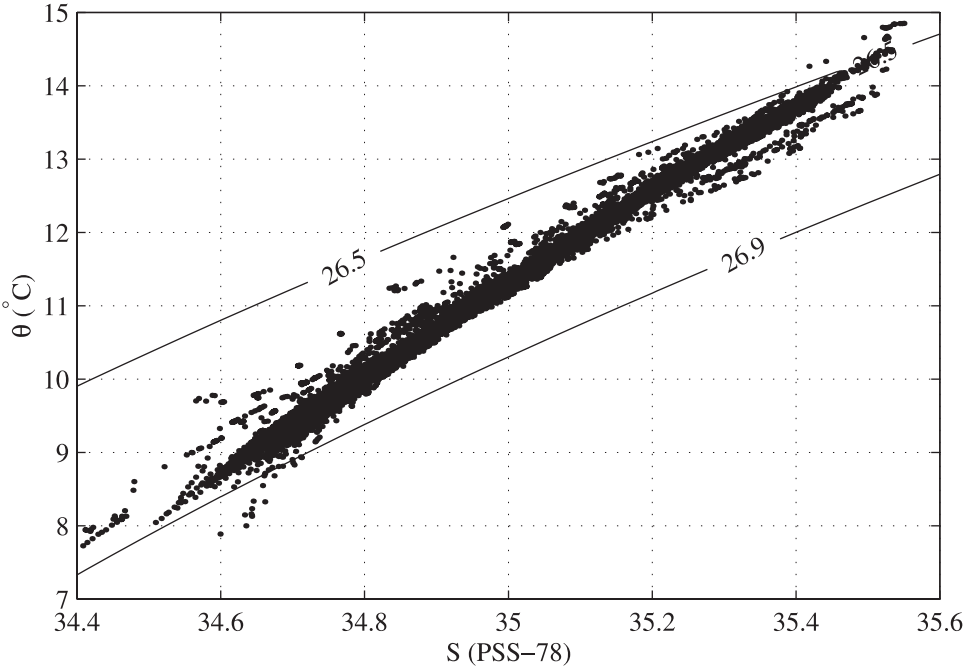

Figure 8. θ-*S* plot of South Indian Ocean SAMW according to Argo profiles. Contours of $\sigma_\theta = 26.5$ and 26.9 kg m^{-3} are superimposed.

In the Subantarctic Zone, SAMW was present continuously (in space) in the Argo data set east of 50E. On the minimum PV surface, it had progressively higher densities towards the east: densities lighter than $\sigma_\theta = 26.7$ kg m^{-3} west of 80E, intermediate densities $\sigma_\theta =$ 26.7 to 26.8 kg m^{-3} between 80 and 100E, and densities greater than $\sigma_\theta = 26.8$ kg m^{-3} east of 100E (Fig. 9). Therefore, with distance eastward, increasingly colder, fresher, and denser SAMW were injected into the South Indian Ocean subtropical gyre from the Subantarctic Zone east of 50E. Karstensen and Quadfasel (2002) have found that lateral transfer along the SAF and the STF was responsible for injecting mode water of densities 26.5 to 26.9 kg m^{-3} in the South Indian Ocean. No SAMW was observed in the Subantarctic Zone west of 50E. This may be due to sparsity of Argo data in that area, or it may be that SAMW formation is not spatially continuous in the Subantarctic Zone.

Following the spread of SAMW θ-*S* properties and their corresponding densities on the minimum PV surface (Fig. 9), it can be deduced that SAMW in the South Indian Ocean spreads northeastward from the Subantarctic Zone east of 50E into the subtropical gyre to about 35S, then northwestward toward the equator. This pattern qualitatively agrees with the flow field in Figure 5. Lighter SAMW ($\sigma_\theta < 26.7$ kg m^{-3}) was confined to the recirculation gyre west of 80E. Denser SAMW ($\sigma_\theta > 26.7$ kg m^{-3}) was spread around the outer northeastern rim of the subtropical gyre. The depths at which the minimum PV in

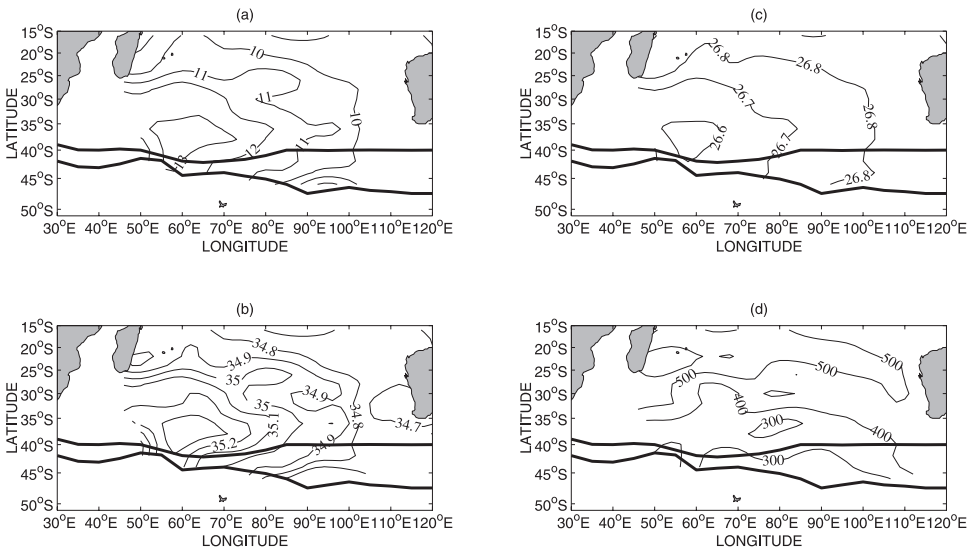

Figure 9. (a) Potential temperature (°C), (b) salinity (PSS-78), (c) potential density (kg m^{-3}), and (d) pressure (dbar), along the surface of minimum potential vorticity in the SAMW layer. Properties have been objectively mapped onto a 2° × 2° grid. The two thick lines mark the locations of STF and SAF.

SAMW were found in the Argo data set (Fig. 9d) agreed with the depths at which an intermediate-depth oxygen maximum was observed in the South Indian Ocean subtropical gyre (along 18S in Warren (1981), along 32S in Toole and Warren (1993)). West of 45E, SAMW in the Argo data set was weak and variable. Hence SAMW properties there are not shown in Figure 9.

Some of the densest SAMW in the northeastern rim of the subtropical gyre could have an origin in the Subantarctic Zone farther east than the present data set. Thompson and Edwards (1981) have observed formation of SAMW south of Tasmania along 145E, with temperature close to 8.6°C, salinity about 34.55, and density 26.85 kg m^{-3}. Davis' (2005) streamfunction map for the South Indian Ocean circulation at 900 m shows the SIOC/ACC flowing as far east as south of Tasmania before retroflecting northwestward back into the South Indian Ocean. This retroflection could transport dense SAMW formed south of Tasmania northwestward into the South Indian subtropical gyre, along the west coast of Australia. On the other side of the basin, SAMW observed at the western boundary along 32S was believed to be old SAMW advected southward by the Agulhas Current (Toole and Warren, 1993). By using a linear oxygen/CFC mixing model, Karstensen and Tomczak (1997) have deduced an age of 5 years for SAMW near 114E, and 25 years at 50E, along 32S.

The thickness of SAMW in the subtropical gyre (Fig. 10) reflects the thickness of the winter mixed layer in the local Subantarctic Zone, as well as the circulation of SAMW.

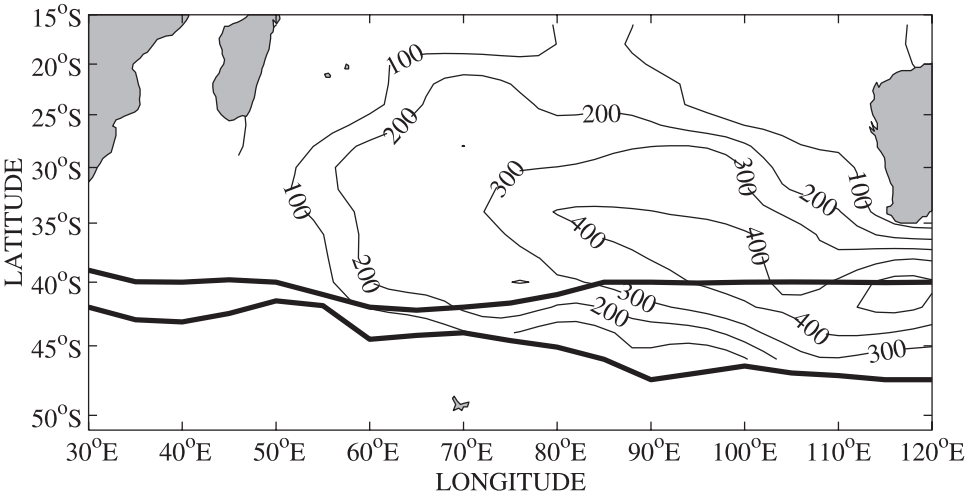

Figure 10. Thickness (dbar) of the SAMW layer in the South Indian Ocean, according to the Argo data set.

South of 35S, the SAMW layer was in general thicker than 400 dbar east of 80E, and thinner than 400 dbar west of 80E. This corresponds to the distribution of winter mixed layer thickness in the local Subantarctic Zone (Fig. 6d). North of 35S, SAMW thickness decreases toward the equator, signifying the gradual erosion of the potential vorticity signature by mixing, as SAMW spreads equatorward. Along the west coast of Australia, SAMW presumably has an origin south of Australia, and has been transported northwestward into the South Indian Ocean by the SIOC/ACC retroflection. Its distance from its remote source may explain the thinness of the SAMW layer along the west coast of Australia. Similarly, the weak SAMW west of 50E could be due to its being old SAMW advected southward by the Agulhas Current.

SAMW is increasingly colder, fresher, and denser with distance east (Fig. 11), as has been observed in previous studies. However, according to the Argo profiles, the longitudinal property variation of SAMW was more continuous and regular than previously observed (e.g. McCartney, 1982; Toole and Warren, 1993; Fine, 1993). The minimum SAMW density at each longitude increased almost linearly with distance east, from 26.5 kg m^{-3} at 60E, to 26.8 kg m^{-3} at 110E. South Indian Ocean SAMW observed in the Argo data set is therefore more continuous in geographical and density space than previously described. This finding may be due to the broad spatial coverage and seasonally unbiased sampling of the Argo profiles, relative to single-line hydrographic surveys.

5. Antarctic Intermediate Water in the South Indian Ocean

Since AAIW is apparent as a vertical salinity minimum in the subtropical gyre, on a θ-S curve it is identifiable as the layer where the stability ratio $R_\rho = \alpha\theta_z/\beta S_z$ changes from

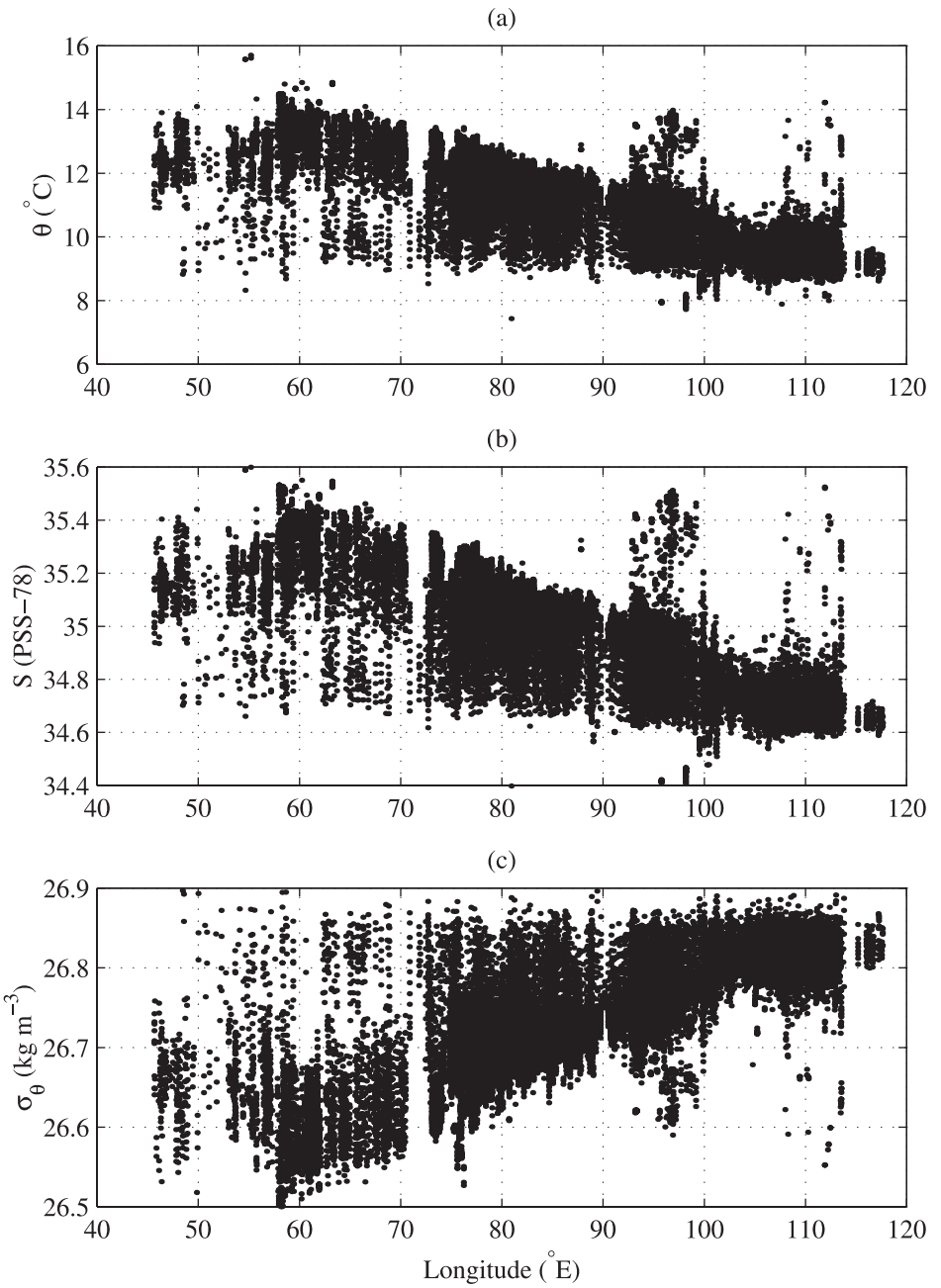

Figure 11. Longitude versus properties of South Indian Ocean SAMW. (a) Potential temperature (°C). (b) Salinity (PSS-78). (c) Potential density (kg m^{-3}).

$R_\rho > 1$ to $R_\rho < 0$. (Strictly speaking, at the absolute salinity minimum, $R_\rho = \infty$.) Here, α is the thermal expansion coefficient, and β is the haline contraction coefficient. The spatial extent of AAIW in the subtropical South Indian Ocean has therefore been identified by where the θ-S curve shows a turning point (i.e. a vertical salinity minimum) below 250 dbar. AAIW extends equatorward from north of the Antarctic Polar Front (not identified in this study but lies generally south of 50S), throughout the subtropical gyre, to as far as the northern extent of the present data set.

Calculation of turning points on the θ-S curves from all Argo profiles showed that the vertical salinity minimum associated with AAIW occurred around $\sigma_\theta = 27.2$ kg m^{-3} in the subtropical South Indian Ocean. Therefore $\sigma_\theta = 27.2$ kg m^{-3} has been treated as the core density surface for South Indian Ocean AAIW. The AAIW core deepened from its outcrop near the Polar Front, and attained its maximum depth (>1100 dbar) at 30–40S and west of 70E (Fig. 12a). From there, it shoaled equatorward and eastward.

Along the core of AAIW, the lowest salinity (<34.4) was found poleward of 30S and east of 55E (Fig. 12b). In the latitude band 30 to 40S, AAIW salinity distribution on density surfaces east of 55E had the smallest meridional gradients in the South Indian Ocean (approx. 0.05 psu over 10° of latitude on $\sigma_\theta = 27.2$ kg m^{-3}). In other words, AAIW's low salinity signature is subjected to minimal mixing there. At similar latitudes but west of 55E, AAIW salinity was higher, due to mixing with warm, high-salinity water from the Red Sea being transported south (Warren, 1981; Toole and Warren, 1993; Fine, 1993). North of 30S, AAIW properties were modified through mixing during its equatorward advection, and so both temperature and salinity increased equatorward.

Along 32S, Toole and Warren (1993) and Fine (1993) have described longitudinal variations in AAIW properties in details. To investigate longitudinal variations in other latitude bands in the subtropical gyre, salinity in the density range 27.0–27.5 kg m^{-3} have been averaged from Argo profiles in 5° × 5° boxes between 15–40S, 30–120E (Fig. 13). The density range 27.0–27.5 kg m^{-3} was chosen following the analysis of Toole and Warren (1993).

The relatively high salinity in AAIW along the western boundary can be seen south of 25S, with the highest averaged value of 34.58 found in the latitude band 25–30S, off the coast of South Africa (Fig. 13c). Salinity then gradually decreased towards the east. In the latitude band 30–35S, averaged salinity at 60–75E (Crozet Basin) was lower than that at 100–115E (Perth Basin) by 0.02 psu. This difference in averaged salinity between the two basins has been observed by Toole and Warren (1993) along 32E, who also noted that corresponding dissolved oxygen values were higher in the Crozet Basin than in the Perth Basin. The combination of low salinity and high dissolved oxygen contents indicates that AAIW in the Crozet Basin has a more recent origin than in the Perth Basin. Toole and Warren (1993) deduced that AAIW was injected into the South Indian Ocean subtropical gyre in mid-basin. Indeed, Stramma and Lutjeharms (1997) have proposed that the narrow Subantarctic Zone between 60 and 80E could be an area of possible exchanges between the ACC and the South Indian Ocean subtropical gyre. Fine (1993) also concluded that along

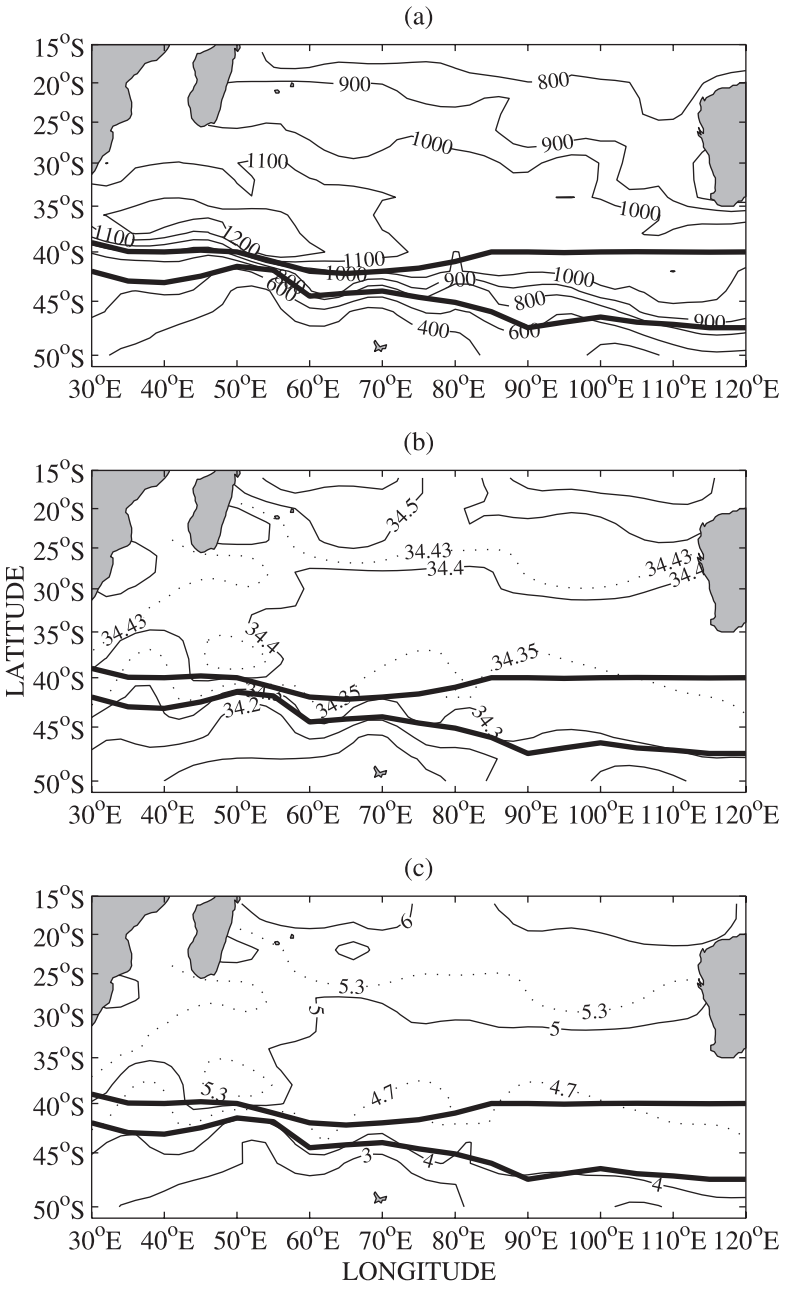

Figure 12. Properties of AAIW on $\sigma_\theta = 27.2$ kg m^{-3} in the South Indian Ocean, according to Argo profiles. (a) Pressure (dbar). (b) Salinity (PSS-78). (c) Potential temperature (°C). Properties have been objectively mapped onto a 2° × 2° grid.

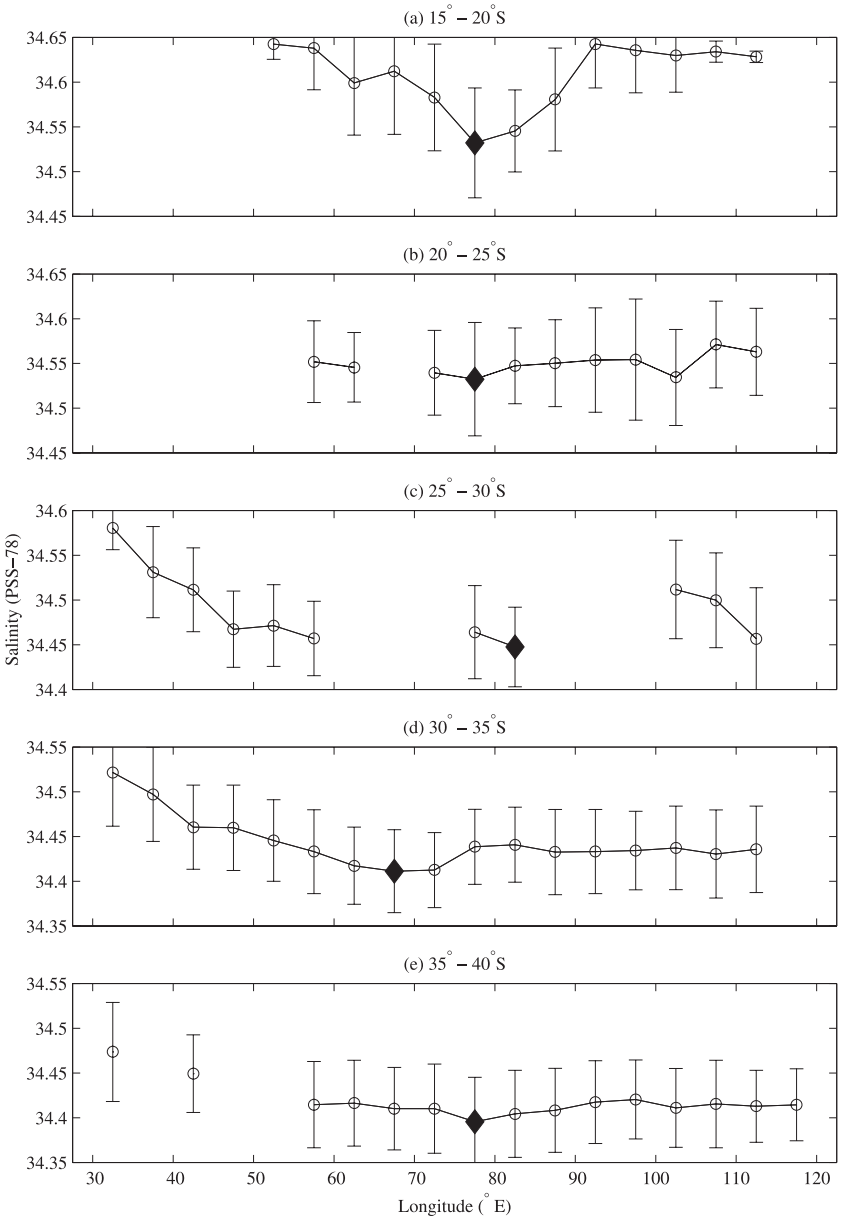

Figure 13. Averaged salinity (PSS-78) in AAIW between 27.0 and 27.5 kg m^{-3}, from Argo profiles in 5° × 5° boxes between 15–40S, 30–120E. Different salinity ranges have been used to show details more clearly, but each range has been fixed to span 0.2 psu. Solid ◆ marks the lowest averaged salinity in each latitude band. Error bars indicate standard deviation within each box.

32S, the most recently ventilated AAIW was confined to the recirculation gyre west of 72E, with the Agulhas Current impeding equatorward advection of AAIW along the western boundary. AAIW in the eastern basin may have had a longer pathway to the South Pacific first, before retroflecting westward into the eastern South Indian Ocean. An apparent age of 9 years was given to AAIW at 60–64E, and 30 years for AAIW east of 72E (Fine, 1993).

The acceleration potential map on $\sigma_\theta = 26.5$ kg m^{-3} (Fig. 5) indicates that northward flow is present at intermediate depths between 65E and 85E. In each latitude band, the lowest averaged salinity in AAIW was also found at the same longitudes 65–85E, with the mid-basin low salinity signature being most striking in the latitude band 15–20S (Fig. 13a). Thus the Argo data set also supports a mid-basin pathway for northward transport of fresh AAIW. The surprising feature revealed by the Argo profiles was that this northward penetration extended as far as the northern extent of the present data set. Based on salinity-oxygen extrema and geopotential topography at 100 dbar, Warren (1981) has inferred relatively intense northward flow between 75 and 100E for the upper waters along 18S. However, a northward flow at intermediate depths along 18S was not noted. So the relatively strong low salinity signature of AAIW in mid-basin in the latitude band 15–20S suggested by the Argo data is striking.

6. Summary and discussion

The purpose of this study is two-fold. The first part of this study demonstrates how effective quality control on sensor drift can be carried out in float salinity measurements by comparing float data time series against background climatology, using methods such as that of Wong *et al.* (2003). Then by using quality-controlled neighboring profiles and the tightest part of the θ-S curve, the noise estimate from the float measurements should reflect very little natural variability, and should contain mostly instrument noise. This noise estimate can therefore be used as an estimate of measurement accuracy. The accuracy of the selected Argo salinity data set in the South Indian Ocean has been estimated to be better than 0.01 psu. Such accuracy is sufficient for many large-scale ocean studies.

The second part of this study exploits the well-dispersed Argo profiles in the South Indian Ocean to survey the contemporary basin-wide properties of SAMW and AAIW. The seasonally unbiased nature of autonomous float measurements also allows water mass characteristics to be studied in relation to winter mixed layer properties. The basin-wide pictures given by the Argo floats generally agree with previous descriptions of SAMW and AAIW in the South Indian Ocean based on single-line hydrographic surveys (Warren, 1981; Fine, 1993; Toole and Warren, 1993).

South Indian Ocean SAMW occupies the density range 26.5 to 26.9 kg m^{-3}. In the Argo data set, it is more continuous in geographical and density space than previously described. It is injected into the subtropical gyre from the Subantarctic Zone east of 50E at increasing densities and thickness toward the east, in accordance with properties of the winter mixed layer in the Subantarctic Zone. It is not clear why the winter mixed layer in the Subantarctic

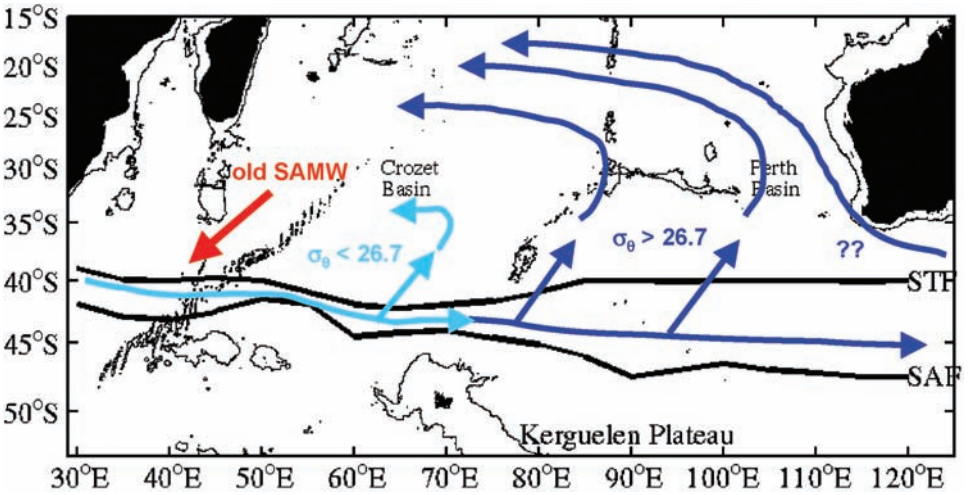

Figure 14. Schematic showing the inferred spreading pathway of South Indian Ocean SAMW. Formation of SAMW and its subsequent injection into the subtropical gyre is continuous from the local Subantarctic Zone.

Zone deepens east of 80E, where the Subantarctic Zone widens east of the Kerguelen Plateau. This increase in winter mixed layer thickness leads to the injection of a thick layer of SAMW of densities greater than 26.7 kg m^{-3} into the eastern South Indian Ocean, which is then spread anticlockwise around the outer northeastern rim of the subtropical gyre (Fig. 14). Some of the densest SAMW along the west coast of Australia could have an origin south of Australia. On the other side of the basin east of South Africa, SAMW is older, having been advected south by the Agulhas.

South Indian Ocean AAIW is centered on the density surface $\sigma_\theta = 27.2$ kg m^{-3}. Fresh AAIW is injected into mid-basin along 65–85E, and is transported equatorward by a northward flow that extends to the northern extent of this study region at 15S (Fig. 15). AAIW in the eastern basin is older in apparent age, and may have taken a longer pathway via the South Pacific (Fine, 1993). West of 55E, AAIW has higher salinity due to mixing with Red Sea Water. The latitude band 30–40S east of 55E has the lowest salinity in AAIW, and the smallest meridional salinity gradient on density surfaces in AAIW. This means that the low salinity signature of AAIW is subjected to minimal mixing at that location, which makes it the ideal place in the South Indian Ocean to detect integrated decadal changes in the salinity minimum of AAIW.

It is interesting to contrast the properties of SAMW and AAIW in the South Indian Ocean. While the vertical potential vorticity minimum of SAMW occupies a wide density range, the vertical salinity minimum of AAIW is exceptionally uniform in density. AAIW in the western basin is of a more recent origin, while AAIW in the eastern basin is old (Fine, 1993). On the other hand, SAMW in the eastern basin is a thicker and better defined pycnostad than SAMW in the western basin. While South Indian Ocean SAMW is formed

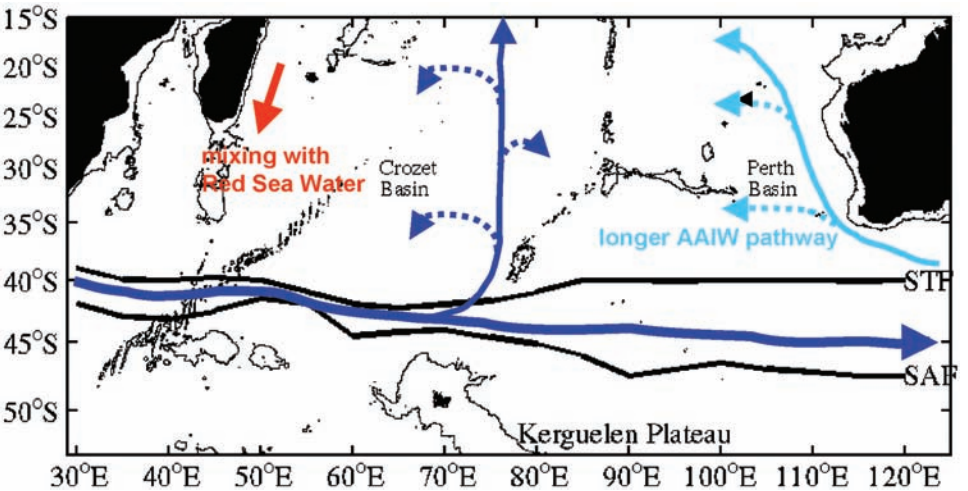

Figure 15. Schematic showing the inferred spreading pathway of South Indian Ocean AAIW. Formation site is not inferred in this study.

in the local Subantarctic Zone, the source of South Indian Ocean AAIW is still debated. These two intermediate-depth water masses in the South Indian Ocean have very different properties, circulation pathways, and source regions. Any temporal change studies on intermediate-depth water masses in the South Indian Ocean should therefore regard changes in SAMW and AAIW separately.

At the time of writing, the Argo data set in the South Indian Ocean was still sparse between 20 and 30S. Upon completion of the array, an exciting prospect is to conduct circumpolar studies of SAMW and AAIW, similar to the work of McCartney (1977) and Piola and Georgi (1982), but at a higher resolution. Another future challenge is to use the Argo data set to investigate decadal changes in SAMW and AAIW in the South Indian Ocean, at higher spatial resolutions than by using repeat single-line surveys.

Acknowledgments. This study was initiated during a visit to Southampton Oceanography Centre in October 2003. I wish to thank Dr. Brian King for the stimulating discussions, and for making available the CTD data from the 2002 32S line repeat in the South Indian Ocean (Charles Darwin cruise 139). The method for detecting sensor drift and offset in float salinity data has been a cumulative effort by many scientists. Comments from two anonymous reviewers greatly improved the manuscript. Argo data were collected and made freely available by the International Argo Project and the national programmes that contribute to it (www.argo.net). This is a publication of the University of Hawaii pursuant to National Oceanic and Atmospheric Administration Award No. NA17RJ1230. It is JIMAR manuscript number 04-351, PMEL contribution number 2744.

REFERENCES

Bacon, S., L. Centurioni, and W. Gould. 2001. The evaluation of salinity measurements from PALACE floats. J. Atmos. Oceanic Tech., *18,* 1258–1266.

Banks, H., R. Wood, J. Gregory, T. Johns and G. Jones. 2000. Are observed decadal changes in

intermediate water masses a signature of anthropogenic climate change? Geophys. Res. Lett., *27,* 2961–2964.

Bryden, H., E. McDonagh and B. King. 2003. Changes in ocean water mass properties: oscillations or trends? Science, *300,* 2086–2088.

Centurioni, L. and J. Gould. 2004. Winter conditions in the Irminger Sea revealed by profiling floats. J. Mar. Res., *62,* 313–336.

Conkright, M. *et al*. 2002. World Ocean Database 2001, Volume 1: Introduction, Sydney Levitus, ed., NOAA Atlas NESDIS 42, U.S. Government Printing Office, Washington, DC, 167 pp.

Davis, R. 2005. Intermediate-depth circulation of the Indian and South Pacific oceans measured by autonomous floats. J. Phys. Oceanogr., *35*, 683–707.

Fine, R. 1993. Circulation of Antarctic Intermediate Water in the South Indian Ocean. Deep-Sea Res., *40,* 2021–2042.

Fukumori, I. and C. Wunsch. 1991. Efficient representation of the North Atlantic hydrographic and chemical distributions. Prog. Oceanogr., *27,* 111–195.

Gordon, A., J. Lutjeharms and M. Gründlingh. 1987. Stratification and circulation at the Agulhas Retroflection. Deep-Sea Res., *34,* 565–599.

Gould, J. *et al*. 2004. Argo profiling floats bring new era of *in situ* ocean observations. EOS, *85,* 185.

Hanawa, K. and L. Talley. 2001. Mode waters, *in* Ocean Circulation and Climate—Observing and Modelling the Global Ocean, G. Siedler, J. Church, and J. Gould, eds., Academic Press, 373–386.

Karstensen, J. and D. Quadfasel. 2002. Formation of southern hemisphere thermocline waters: water mass conversion and subduction. J. Phys. Oceanogr., *32,* 3020–3038.

Karstensen, J. and M. Tomczak. 1997. Ventilation processes and water mass ages in the thermocline of the southeast Indian Ocean. Geophys. Res. Lett., *24,* 2777–2780.

McCartney, M. 1977. Subantarctic Mode Water, *in* A Voyage of Discovery, M. V. Angel, ed., Deep-Sea Res., *24* (Suppl.), 103–119.

—— 1982. The subtropical recirculation of mode waters. J. Mar. Res., *40* (Suppl.), 427–464.

McDonagh, E., H. Bryden, B. King, R. Sanders, S. Cunninghan and R. Marsh. 2005. Decadal changes in the South Indian Ocean thermocline. J. Climate, *18*, 1575–1590.

Molinelli, E. 1981. The Antarctic influence on Antarctic Intermediate Water. J. Mar. Res., *39,* 267–293.

Olson, D., R. Fine and A. Gordon. 1992. Convective modifications of water masses in the Agulhas. Deep-Sea Res., *39* (Suppl.), S163–S181.

Orsi, A., T. Whitworth III and W. Nowlin Jr. 1995. On the meridional extent and fronts of the Antarctic Circumpolar Current. Deep-Sea Res., *42,* 641–673.

Phillips, H., S. Wijffels and M. Feng. 2005. Interannual variability in the freshwater content of the Indonesian-Australian Basin. Geophys. Res. Lett., *32,* L03,603, doi:10.1029/2004GL021,755.

Piola, A. and D. Georgi. 1982. Circumpolar properties of Antarctic Intermediate Water and Subantarctic Mode Water. Deep-Sea Res., *29,* 687–711.

Reid, J. 1965. Intermediate Waters of the Pacific Ocean, The Johns Hopkins Oceanographic Studies Number 2, The Johns Hopkins Press. Baltimore, 85 pp.

Sloyan, B. and S. Rintoul. 2001. Circulation, renewal, and modification of Antarctic mode and intermediate water. J. Phys. Oceanogr., *31,* 1005–1030.

Stramma, L. 1992. The South Indian Ocean Current. J. Phys. Oceanogr., *22,* 421–430.

Stramma, L. and J. Lutjeharms. 1997. The flow field of the subtropical gyre of the South Indian Ocean. J. Geophys. Res., *102*(*C3*), 5513–5530.

Talley, L. 1996. Antarctic Intermediate Water in the South Atlantic, *in* The South Atlantic: Present and Past Circulation, G. Wefer *et al.,* eds., Springer, 219–238.

Talley, L. 1999. Some aspects of ocean heat transport by the shallow, intermediate and deep overturning circulations, *in* Mechanisms of Global Climate Change at Millennial Time Scales,

P. U. Clark, R. S. Webb and L. D. Keigwin, eds., American Geophysical Union, Washington, DC, Geophys. Mono. Ser. *112,* 1–22.

Thompson, R. and R. Edwards. 1981. Mixing and water-mass formation in the Australian Subantarctic. J. Phys. Oceanogr., *11,* 1399–1406.

Toole, J. and B. Warren. 1993. A hydrographic section across the subtropical South Indian Ocean. Deep-Sea Res., *40,* 1973–2019.

Warren, B. 1981. Trans-Indian hydrographic section at lat.18°S: property distributions and circulation in the South Indian Ocean. Deep-Sea Res., *28A,* 759–788.

Wong, A., G. Johnson and W. Owens. 2003. Delayed-mode calibration of autonomous CTD profiling float salinity data by θ-*S* climatology. J. Atmos. Oceanic Tech., *20,* 308–318.

Received: *31 August, 2004;* revised: *21 April, 2005.*